

# Matching resummed endpoint and continuum $\gamma$ -ray spectra from dark-matter annihilation

M. BENEKE<sup>a</sup>, K. URBAN<sup>a</sup>, and M. VOLLMANN<sup>b</sup>

<sup>a</sup>*Physik Department T31,  
James-Franck-Straße 1, Technische Universität München,  
D-85748 Garching, Germany*

<sup>b</sup>*Institut für Theoretische Physik,  
Auf der Morgenstelle 14, Eberhard Karls Universität Tübingen,  
72076 Tübingen, Germany*

## Abstract

For the minimal wino and Higgsino benchmark models we provide accurate energy spectra of high-energy photons from TeV scale dark-matter annihilation  $\chi\chi \rightarrow \gamma + X$  by merging electroweak Sudakov resummation near maximal energy with the electroweak parton-shower PPC4DM, and accounting for the Sommerfeld effect. Electroweak resummation significantly changes the shape of the photon-energy spectrum in the wide range  $E_\gamma \sim (0.6 \dots 1) m_\chi$  and hence the form of the so-called “line-signal”.

# 1 Introduction

The properties of dark matter (DM) beyond its gravitational interaction is one of the biggest open questions of particle physics and cosmology today. Even though not detected so far, weakly interacting massive particles (WIMPs) remain among the most promising candidates for particle DM, especially if connected to the electroweak scale as, e.g., in supersymmetric models [1], or due to their minimal model assumptions [2, 3]. The two obvious benchmark scenarios for such TeV electroweak WIMPs are the pure wino and Higgsino. Their thermal masses are in the (1 – 3) TeV region [4, 5], and a discovery or exclusion is out of reach for current collider experiments [6]. It is also not clear if future possible collider experiments will exclude or discover the wino and Higgsino conclusively [7]. The situation is comparably grim for nuclear scattering given cross sections near or within the coherent neutrino background in direct detection experiments [8]. However, the indirect detection of a TeV WIMP DM annihilation signal in cosmic rays offers a way to challenge these models with current and upcoming experiments [9, 10].

One of the most sensitive indirect detection probes is the  $\gamma$ -ray line signal. However, only including the line-signal  $\chi\chi \rightarrow \gamma\gamma + \frac{1}{2}\gamma Z$  into the analysis is too naive. The precise prediction of the expected DM signal is complicated by several effects. First, since the DM is electrically neutral, the annihilation into photons is only possible through loop processes [11–13], and more importantly, via mixing with a slightly heavier charged multiplet partner through the Sommerfeld effect [14–16]. The latter enhances the cross section by up to several orders of magnitude and is itself subject to large electroweak (EW) corrections [5, 17, 18]. Second, the large ratio of DM mass to the EW gauge boson masses together with the semi-inclusive ( $\gamma + X$ ) nature of detecting a photon at earth [19, 20] leads to large Sudakov double logarithms  $\ln^2(4m_\chi^2/m_W^2)$  that require resummation [21–25]. On top, the finite energy resolution, which in the TeV regime for typical Cherenkov telescopes is of order several percent of the DM mass  $m_\chi$ , induces further large logarithms of the energy resolution vs. DM mass and/or electroweak scale [19, 20, 26–28].

The anticipated large energy bins make it imperative to consider the full spectrum beyond the nominal endpoint at which Sudakov resummation is most important. The purpose of this letter is to demonstrate how the endpoint spectra can be utilized and merged with dedicated parton-shower calculations (in this paper PPC4DM [29]) away from the endpoint to obtain realistic predictions for the “photon line-signal” with state-of-the-art theoretical precision. To this end, we investigate the logarithmic structure of resummed and parton-shower spectra and demonstrate which logarithms are correctly captured by either calculation beyond their naive region of validity. With these insights at hand, we devise a merging procedure, thereby providing differential spectra close and away from the endpoint. The logarithmic analysis is not restricted to wino and Higgsino DM but applies to all TeV EW WIMPs, in particular, the minimal DM candidates [2, 3] or even the full MSSM [30]. Additionally, we provide the code `DM $\gamma$ Spec` ancillary to this paper that supplies ready-to-use  $\gamma$ -spectra, which include Sommerfeld and Sudakov resummation to next-to-leading order (NLO), respectively NLL’ (NLL + NLO), for wino

and Higgsino DM, merged with PPPC4DM spectra away from the endpoint. Details on the code (and download information) and the merging procedure is provided in the appendices to the main text.

## 2 Endpoint spectrum resummation

The main focus of this paper lies on the exemplary pure wino and Higgsino DM models, that produce the observed relic density with a thermal mass of  $m_\chi = 2.842$  TeV [5] and  $m_\chi = 1.1$  TeV, respectively. The former is an  $SU(2)_L$  triplet of Majorana fermions with a mass difference of  $\delta m_\chi = 164.1$  MeV between the charged and neutral states of the multiplet [31, 32]. The Higgsino is an  $SU(2)_L$  doublet of Dirac fermions with hypercharge, that splits into two neutral Majorana fermions  $\chi_1^0$  and  $\chi_2^0$  with a mass difference  $\delta m_N \geq 150$  keV, that we fix to  $\delta m_N = 20$  MeV for figures in this paper, and a charged component of the multiplet, that is  $\delta m_\chi \approx 355$  MeV heavier [33]. In both models, the detection of a line signal becomes possible, as the neutral DM particles can convert into a pair of charged virtual states before annihilation via the exchange of EW gauge bosons, commonly known as Sommerfeld effect [3, 14, 15]. The EW potentials are known to NLO for the Higgsino [18] and wino [5, 17], and are included to this accuracy in this work.

In indirect detection of the photon signal, the observable is not the literal line signal, i.e., annihilation to  $2\gamma\gamma + \gamma Z$ , but rather  $\chi^0\chi^0 \rightarrow \gamma + X$ , where the unobserved final state  $X$  is kinematically constrained to be jet-like by the finite energy resolution of the detector [20]. Additionally, for TeV DM masses, the hierarchy between DM and EW scale masses  $m_\chi \gg m_W$  induces large Sudakov double logarithms. The small quantities associated with these large logarithms are

$$\epsilon = \frac{m_W}{2m_\chi}, \quad 1 - x = 1 - \frac{E_\gamma}{m_\chi} \quad (1)$$

with  $E_\gamma$  the energy of the detected photon. The resummation of these large logarithms is achieved in the framework of soft-collinear effective theory (SCET) [34–36]. Depending on the relative scaling of  $1 - x$  and  $\epsilon$ , different treatments are needed to describe the differential spectrum near the endpoint  $x = 1$ . Resummed results are available for:

- line signal only ( $\gamma + X = 2\gamma\gamma + \gamma Z$ ) — (wino to NLL' [24, 25])
- narrow resolution  $1 - x \sim \epsilon^2$  — (wino [20, 27] and Higgsino [28] to NLL')
- intermediate resolution  $1 - x \sim \epsilon$  — (wino [27] and Higgsino [28] to NLL')
- wide resolution  $1 \gg 1 - x \gg \epsilon$  — (wino to NLL [19, 26])

where LL, NLL refer to the resummation of the leading, respectively, next-to-leading logarithms. The NLL' approximation, in addition, includes the full one-loop corrections.

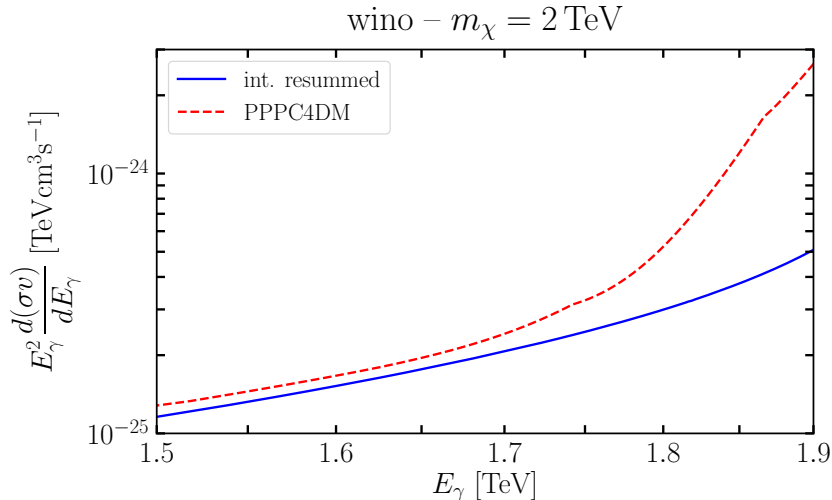


Figure 1: Intermediate resolution resummed (blue/solid) and PPC4DM (red/dashed) gamma spectrum for wino annihilation with mass  $m_\chi = 2$  TeV.

The line signal-only case is contained in the narrow resolution calculation by taking the limit  $x \rightarrow 1$  and decoupling the light fermions. All results can be cast into the form

$$\frac{d(\sigma v)}{dE_\gamma} = 2 \sum_{I,J} S_{IJ} \Gamma_{IJ}^{\text{res}}, \quad (2)$$

where the sum over  $I, J$  runs over the two-particle states that mix with  $\chi^0 \chi^0$  via Sommerfeld enhancement,  $S_{IJ}$  encapsulates the Sommerfeld enhancement and  $\Gamma_{IJ}^{\text{res}}$  is determined in the respective effective field-theory (EFT) computation.

Given the typical energy resolution of Cherenkov telescopes of several percent of DM mass (e.g., [10]), the bulk of the endpoint spectrum probed lies in the intermediate resolution regime. Here, we are concerned with obtaining a full spectrum beyond the endpoint, and hence consider the merging of the intermediate resolution logarithms to the parton-shower calculation provided in PPC4DM [29]. An example of the spectra using only EFT (intermediate resolution) or only PPC4DM is shown for a 2 TeV wino in Fig. 1, which demonstrates that away from the endpoint, the Sudakov resummed EFT and PPC4DM calculations converge.<sup>1</sup> We define

$$\left. \frac{d(\sigma v)}{dx} \right|_{\text{PPPC4DM}} = 2 \sum_{IJ} S_{IJ} \left( \hat{\Gamma}_{IJ}^{WW} \frac{dN_{WW}}{dx} + \hat{\Gamma}_{IJ}^{ZZ} \frac{dN_{ZZ}}{dx} + \hat{\Gamma}_{IJ}^{\gamma Z} \frac{dN_{\gamma Z}}{dx} + \hat{\Gamma}_{IJ}^{\gamma\gamma} \frac{dN_{\gamma\gamma}}{dx} \right), \quad (3)$$

where  $dN_{AB}/dx$  denote the splitting functions of  $AB$  into  $\gamma + X$ , and  $\hat{\Gamma}_{IJ}^{AB} = (\sigma v)_{\text{tree}}^{IJ \rightarrow AB}$  are the tree-level annihilation matrices. The inclusion of the Sommerfeld enhancement

<sup>1</sup>Towards the endpoint in Fig. 1, the resummed spectrum is suppressed with respect to PPC4DM. Part of this suppression is due to the resummed Sudakov logarithms. In addition, PPC4DM smears the tree-level delta-distribution at the endpoint, which further enhances the difference between the two curves in Fig. 1. For a comparison, including the behaviour at the absolute endpoint of both calculations, see Fig. 4 and the accompanying discussion in Sec. 5.

mandates the consideration of off-diagonal terms such as  $\hat{\Gamma}_{(00)(+-)}^{AB}$ , which mix the different neutral two-particle states. Since the wino and Higgsino are pure multiplets, they only annihilate into EW gauge bosons at tree-level. The Higgs boson and SM fermions enter only at loop-level or via the EW evolution.

### 3 Logarithmic structure of the result

To allow for a comparison of the logarithmic structure between the EFT calculations and PPC4DM, we extend the definition of  $dN/dx$  to the resummed case. Strictly speaking,  $dN/dx$  is only useful within the collinear approximation, which only includes collinear splittings of the two-gauge boson final-state of tree-level annihilation. The resummed calculations on the other hand, also includes model-dependent initial-state radiation (ISR), which cannot be associated with a particular tree-level annihilation matrix. For the purpose of comparison, we nevertheless define

$$\frac{dN_{WW}^{IJ}}{dx} \equiv m_\chi \frac{\Gamma_{IJ}^{\text{res}}}{\hat{\Gamma}_{IJ,\text{tree}}^{WW}} \quad (x < 1) \quad (4)$$

in a slight abuse of notation. We restrict to  $x < 1$  to exclude virtual corrections, which are proportional to  $\delta(1-x)$ , from the comparison, as we are interested in the differential terms in  $x$ .

We investigate the leading terms in the  $\hat{\alpha}_2$  expansion of the two calculations for the wino model.<sup>2</sup> The Sommerfeld term becomes  $S_{IJ} = \delta_{I(00)}\delta_{J(00)}$ , and the right-hand side of (2) reduces to  $\chi^0\chi^0 \rightarrow W^+W^-\gamma$  in the tree approximation. We should mention that this process is numerically subdominant (for TeV scale DM masses) relative to formally higher-order but Sommerfeld-enhanced loop processes such as  $\chi^0\chi^0 \rightarrow \chi^+\chi^- \rightarrow W^+W^-\gamma$  which is of  $\mathcal{O}(\hat{\alpha}_2^5 m_\chi^2/m_W^2)$ . Nevertheless, we begin our investigation with  $\chi^0\chi^0 \rightarrow W^+W^-\gamma$ , as on top of the endpoint-resummed [27] and the collinear-approximation result [29, 37], the full fixed-order computation is also available [38].

The intermediate-resolution endpoint-resummed expression, expanded back in  $\hat{\alpha}_2$  to lowest non-vanishing order, results in the approximation

$$\left. \frac{dN_{WW}}{dx} \right|_{\chi^0\chi^0 \rightarrow WW\gamma}^{\text{int.}} = \frac{2\alpha_{\text{em}}}{\pi} \left[ \frac{1}{1-x} \ln \left( 1 + \frac{(1-x)^2}{\epsilon^2} \right) - \frac{1-x}{\epsilon^2 + (1-x)^2} \right]. \quad (5)$$

This approximation implicitly assumes  $1-x \sim \epsilon \ll 1$ . Similarly, we can extract the corresponding splitting function for PPC4DM following [37], which employs the collinear approximation, and obtain

$$\left. \frac{dN_{WW}}{dx} \right|_{\text{PPC4DM}} = \frac{2\alpha_{\text{em}}}{\pi} \left[ \frac{x}{1-x} \ln \frac{(1-x)^2}{\epsilon^2} - \left( \frac{1-x}{x} + x(1-x) \right) \ln \epsilon^2 \right]. \quad (6)$$

---

<sup>2</sup>Similar considerations hold for the Higgsino model, but the formulas become lengthier due to the additional  $\chi_1^0\chi_1^0 \rightarrow ZZ$  tree-level annihilation term.

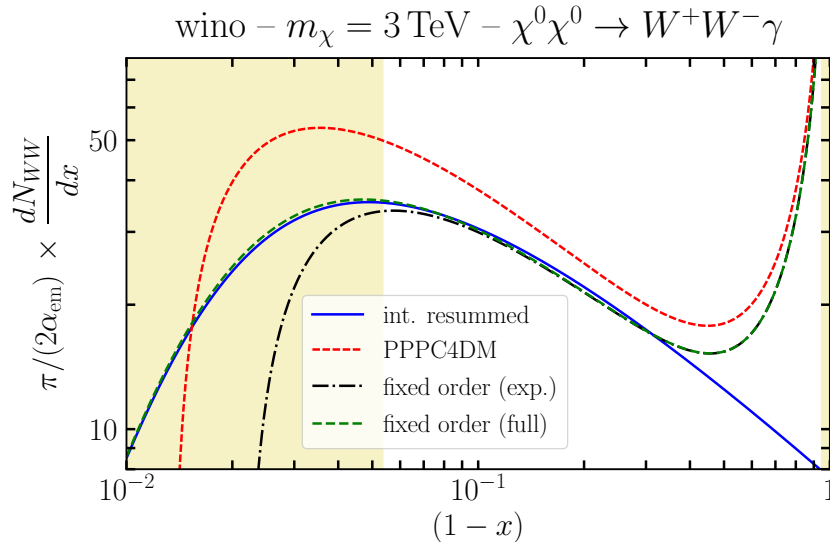


Figure 2: Photon energy spectrum from  $\chi^0 \chi^0 \rightarrow W^+ W^- \gamma$  for a 3 TeV wino ( $\epsilon \approx 0.0134$ ) obtained from (5), (6), (7) and the unexpanded fixed-order result [38]. The shaded areas mark  $1 - x < 4\epsilon$  and  $x < 4\epsilon$ . Note the plot is logarithmic in  $1 - x$ .

The collinear approximation is valid if  $\epsilon \ll 1 - x = \mathcal{O}(1)$ . Finally, we consider the fixed-order unresummed computation [37, 38], expanded in  $\epsilon$  and the mass difference between charged and neutral DM, which yields

$$\begin{aligned} \left. \frac{dN_{WW}}{dx} \right|_{\chi^0 \chi^0 \rightarrow WW\gamma}^{\text{f.o.}} &= \frac{2\alpha_{\text{em}}}{\pi} \left[ \frac{(1-x+x^2)^2}{(1-x)x} \ln \frac{1}{\epsilon^2} \right. \\ &\quad - \frac{(4-12x+19x^2-22x^3+20x^4-10x^5+2x^6)}{(2-x)^2(1-x)x} \\ &\quad \left. + \frac{8-24x+42x^2-37x^3+16x^4-3x^5}{(2-x)^3(1-x)x} \ln(1-x) \right]. \end{aligned} \quad (7)$$

The fixed-order computation is valid whenever no large logarithms appear, i.e. for  $1 - x \gg \epsilon$  and  $x \gg \epsilon$ . Hence, we expect the collinear approximation to match the fixed-order result, for  $1 - x \gg \epsilon$ . Eq. (7) captures model-dependent terms, which are not part of the collinear approximation (6).

In Fig. 2, we show the  $\gamma$ -spectra obtained from (5), (6), and (7) for a wino of mass  $m_\chi = 3 \text{ TeV}$ , together with the unexpanded (in  $\epsilon$ ) fixed-order result [38]. Close to the endpoint, here to the left side of the figure due to the logarithmic plot in  $1 - x$ , the unexpanded fixed-order calculation and the NLL<sup>2</sup>-accurate endpoint result match essentially perfectly inside the left-shaded band, which indicates the region of validity of the latter computation.<sup>3</sup> The collinear approximation (PPPC4DM) fails badly here.

<sup>3</sup>We emphasize that we compare fixed orders in the  $\hat{\alpha}_2$  expansion. In the left-shaded band, higher-

In the transition region  $1 - x \lesssim 0.3$ , fixed-order and the NLL' endpoint approximation still match well. The collinear approximation (6) is about 20% larger than the exact one in the region  $0.1 \lesssim 1 - x \lesssim 0.9$ , where it should be merged to the endpoint-resummed approximation. In the final merged spectra presented below, this discrepancy in a subdominant channel is not a visible effect.

To emphasize the structural dependence on the leading logarithms, we define  $1 - x = \beta\epsilon$ , where  $\beta$  is a fixed constant, such that we can expand all formulas for small  $\epsilon$ . Doing so, yields for the leading  $\epsilon^{-1}$  term

$$\frac{dN_{WW}}{dx} = \frac{2\alpha_{\text{em}}}{\pi} \frac{1}{\epsilon} \left\{ \begin{array}{ll} \frac{\ln(1+\beta^2)}{\beta} - \frac{\beta}{1+\beta^2} & \text{int. res.} \\ \frac{\ln \beta^2}{\beta} & \text{PPPC4DM} \\ \frac{\ln \beta^2 - 1}{\beta} & \text{full fixed order} \end{array} \right\} + \mathcal{O}(\epsilon^0). \quad (8)$$

As evident, for large  $\beta$ , the three approximations have the same leading behaviour, which is expected for the collinear approximation with respect to the full fixed-order computation. However, for the resummed endpoint result, this was not necessarily expected, as large  $\beta$  violates the intermediate resolution scaling  $1 - x \sim \epsilon$  for which (5) was derived. Furthermore, NLL' resummed and fixed order also yield the same non-logarithmic term at large  $\beta$ , which is not part of the collinear approximation, as it stems from model-dependent terms.

Turning to the charged wino annihilation process  $\chi^+\chi^- \rightarrow \gamma + X$ , which is in fact the more important one (due to the Sommerfeld enhancement), the relevant final states are  $X = W^+W^-, f\bar{f}, Zh$ . In the collinear approximation, the  $W^+W^-\gamma$  final state is produced by the same universal  $W \rightarrow W\gamma$  splitting function, hence (6) applies for  $\chi^+\chi^-$  annihilation as well. On the other hand, extracting the  $\chi^+\chi^- \rightarrow W^+W^-\gamma$  process at lowest order from the resummed endpoint calculation gives

$$\begin{aligned} \left. \frac{dN_{WW}}{dx} \right|_{\chi^+\chi^- \rightarrow WW\gamma}^{\text{int.}} &= \frac{2\alpha_{\text{em}}}{\pi} \left[ -\frac{1-x}{\epsilon^2 + (1-x)^2} - \frac{3}{(1-x)} \ln \left( 1 + \frac{(1-x)^2}{\epsilon^2} \right) \right. \\ &\quad \left. - \left( 4 \ln \epsilon^2 + \frac{29}{8} \right) \left[ \frac{1}{1-x} \right]_+ + 4 \left[ \frac{\ln(1-x)}{1-x} \right]_+ \right]. \end{aligned} \quad (9)$$

The plus-distributions regulate the limit  $x \rightarrow 1$ , and are taken care of together with the virtual contributions in the nominal zero-bin at the absolute endpoint, discussed in Appendix A.2. Since our ultimate goal is to provide a merged spectrum from the endpoint  $x = 1$  to  $x \rightarrow 0$ , we are particularly interested in the region in between  $1 - x \gg \epsilon$ , where (6) applies, and  $1 - x \sim \epsilon$ , where (9) is valid. To this end, we expand (9) for small  $\epsilon$ , and (6) in small  $1 - x$  to obtain

$$\left. \frac{dN_{WW}}{dx} \right|_{\chi^+\chi^- \rightarrow WW\gamma}^{\text{int., } \epsilon \rightarrow 0} = \frac{2\alpha_{\text{em}}}{\pi} \frac{1}{1-x} \left[ \ln \frac{1}{\epsilon^2} + \ln \frac{1}{(1-x)^2} - \frac{37}{8} \right] + \mathcal{O}(\epsilon^2), \quad (10)$$

---

order corrections and large, and endpoint-resummation is essential. Similarly, in the right shaded band,  $x < 4\epsilon$ , the fixed-order approximation is inaccurate.

$$\left. \frac{dN_{WW}}{dx} \right|_{\text{PPPC4DM}}^{1-x \rightarrow 0} = \frac{2\alpha_{\text{em}}}{\pi} \frac{1}{1-x} \left[ \ln \frac{1}{\epsilon^2} - \ln \frac{1}{(1-x)^2} \right] + \mathcal{O}((1-x)^0). \quad (11)$$

As expected, the collinear approximation does not produce the correct logarithms as  $x \rightarrow 1$ , but the different sign between the  $\ln(1-x)^{-2}$  terms ensures that the two splitting functions (6) and (9) intersect each other around  $1-x \sim 0.3$ . Furthermore, for large DM masses, i.e. small  $\epsilon$ , the  $\ln \epsilon^{-2}$  term ensures that the shape of both curves is similar in the region between  $1-x \sim \epsilon$  and  $1-x \gg \epsilon$ . We employ a linear merging procedure between the two spectra, as detailed in Appendix A.1. Given the interplay of various terms due to the Sommerfeld enhancement factors, a full assessment of the merging quality is possible only for the full expressions for  $dN/dx$  without expansion in  $\hat{\alpha}_2$ , see the following section.

The other two final states  $\gamma f \bar{f}, \gamma Zh$  contribute

$$\left. \frac{d(\sigma v)}{dx} \right|_{\chi^+ \chi^- \rightarrow \gamma f \bar{f}, \gamma Zh} = (\sigma v)_{\chi^+ \chi^- \rightarrow 2\gamma\gamma + \gamma Z} \frac{\hat{\alpha}_2}{\pi} \left[ \frac{1}{1-x} \right]_+ \left( 1 + \frac{1}{48\hat{c}_W^2} \right) \quad (12)$$

to the NLL' endpoint-resummed spectrum. Here  $(\sigma v)_{\chi^+ \chi^- \rightarrow 2\gamma\gamma + \gamma Z} = 2\pi\hat{\alpha}_2\hat{\alpha}_{\text{em}}/m_\chi^2$ , and the expression includes the splitting into all SM fermion pairs and  $Zh$ , respectively, whose masses can be neglected at intermediate resolution. PPC4DM does not include these processes.

## 4 Merged differential spectra

To provide high-resolution fully differential spectra for all values of  $x$ , we merge the narrow resolution resummed calculation with the intermediate resolution resummation, and the latter with PPC4DM. An in-depth investigation of the logarithmic structure of the narrow vs. intermediate resolution resummation to the two-loop order can be found in [27] and will not be repeated here. Technical details on the merging of the three results are given in Appendix A.1. In the following, we discuss the resulting photon energy spectrum for annihilation of a 2 TeV wino and a 1 TeV Higgsino, shown in Fig. 3. The endpoint region  $1-x \rightarrow 0$  is depicted logarithmically to identify the opening of different final-state channels.

Starting from the left, that is, at the endpoint of maximal photon energy, the spectrum to the left of the clearly visible  $\gamma Z$  peak at  $1-x = m_Z^2/(4m_\chi^2)$  is caused by the process  $\chi\chi \rightarrow \gamma f \bar{f}$ , where  $f$  are the SM fermions excluding the top quark. In the resummation calculation, these fermions are taken as massless. The first light-fermion mass effects are expected from the bottom quark at  $1-x = m_b^2/m_\chi^2$ , which is already outside the range shown in the figure. Light-fermion mass effects can be incorporated in a straightforward modification of the narrow resolution result in [20, 27, 28]. We refrain from performing this modification, since the experimental capabilities are by orders of magnitudes away from being able to resolve this effect. The width of the  $\gamma Z$  peak arises from a consistent treatment of the  $Z$ -boson width using Dyson resummation according

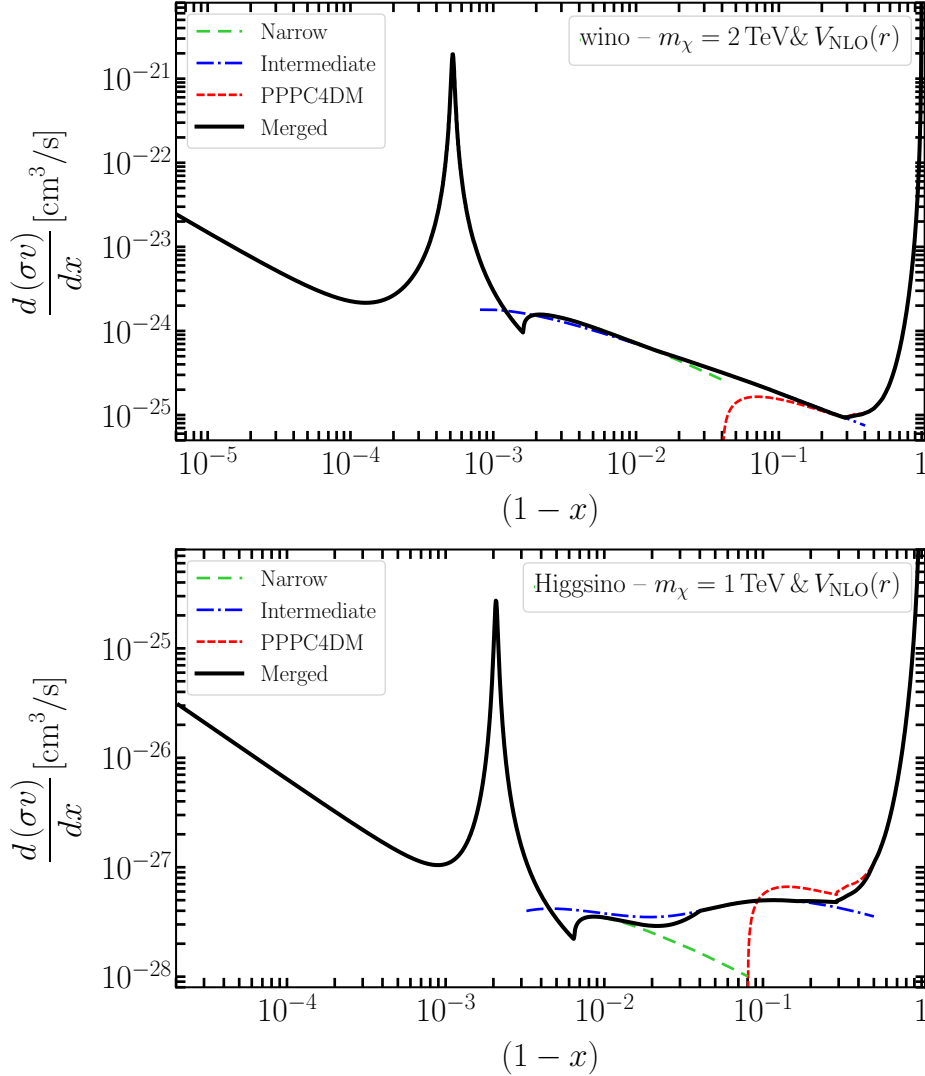


Figure 3: Merged differential spectrum for a 2 TeV-mass wino (upper panel) and Higgsino with  $m_\chi = 1$  TeV (lower panel) with NLO EW potentials and NLL' Sudakov resummation for the endpoint calculations. The merged spectrum is shown in black (solid), whilst the narrow and intermediate resolution calculations are depicted in green (dashed) and blue (dash-dotted), respectively. The PPC4DM result (excluding the smeared  $\delta$ -distributions – see Appendix A.3), is shown in red (short-dashed).

to Eq. (B.59) of [28].<sup>4</sup> To the right of the  $Z$ -peak, we observe a kink at  $1-x = m_W^2/m_\chi^2$  corresponding to the  $\gamma W^+W^-$  threshold opening up, with a collimated  $W^+W^-$  pair. The subsequent  $Zh$  and  $t\bar{t}$  thresholds lie already in the merging region between the nar-

<sup>4</sup>The analogous expressions for hypercharge and mixed hypercharge/SU(2) narrow resolution recoiling jet functions, which are not given in [28], are obtained by the simple replacement of the corresponding couplings and Weinberg angle.

row and intermediate resolution calculation, and would be too weak to be visible on the scale of the plot.

The regime of validity of the intermediate resolution endpoint calculation begins around  $1 - x \sim \frac{m_W}{m_\chi}$ . Here, in addition to all the aforementioned processes, the emission of soft  $W$ -radiation in all directions is kinematically possible. Also, soft initial-state radiation of electroweak gauge bosons becomes possible. At smaller  $1 - x$ , soft effects are purely virtual for kinematic reasons. At  $1 - x \sim 0.3$ , the intermediate resolution calculation is merged with the parton-shower calculation in PPC4DM,<sup>5</sup> which replaces the dedicated endpoint calculations for the remaining part of the spectrum, which as expected, diverges for  $x \rightarrow 0$ , where the photon becomes soft, and the semi-inclusive photon spectrum is no longer observable.

We observe that for all practical purposes, there is an energy region where the two calculations to be merged are sufficiently accurate and in agreement, such that an accurate spectral shape over the entire photon energy range from 0 to  $m_\chi$  is obtained.

## 5 Discussion

Is endpoint resummation important given the present and expected energy resolution of instruments? To address this question, we fold the merged endpoint-accurate spectrum and the PPC4DM-only spectrum with a Gaussian resolution function of energy resolution  $aE_\gamma$ ,

$$\sigma_E(a) \equiv \int_0^{m_\chi} dE'_\gamma \frac{d(\sigma v)}{dE'_\gamma} \cdot \frac{1}{\sqrt{2\pi} \cdot a \cdot E_\gamma} e^{-\frac{(E_\gamma - E'_\gamma)^2}{2 \cdot a^2 \cdot E_\gamma^2}}, \quad (13)$$

and compare the two. The result is shown in Fig. 4 for the 2 TeV wino (upper plot) and 1 TeV Higgsino (lower plot), adopting an energy resolution of  $7\% \times E_\gamma$ , as is expected for CTA in the TeV DM mass regime [10]. The merged spectrum (black/solid) and the PPC4DM prediction omitting endpoint resummation (red/dashed) are shown in the upper panels of the plots. Far away from the endpoint  $E_\gamma = m_\chi$ , the two results agree by construction, since resummation is unimportant. In the endpoint region, however, large deviations can be seen even on the logarithmic scale of the plot, emphasizing the need for resummation. In the subtended panels, the ratio of the resummed, merged spectrum vs. the PPC4DM-only prediction is shown. For the merged spectrum of the wino, there is suppression of the signal relative to PPC4DM till the endpoint and slightly beyond, until at some point the merged spectrum exceeds PPC4DM. The reason for the latter is that PPC4DM smears the tree-level delta-distribution, whilst the EFT computation does not need any smearing, hence the peak of the PPC4DM-only spectrum is pushed to smaller  $E_\gamma$  than the nominal endpoint. The Higgsino spectrum exhibits the same features. In addition, near maximal photon energy, there is also an intricate interplay

---

<sup>5</sup>Note that PPC4DM is used in a modified form to avoid contamination with the smeared tree-level  $\delta$ -distributions. For details, see Appendix A.3.

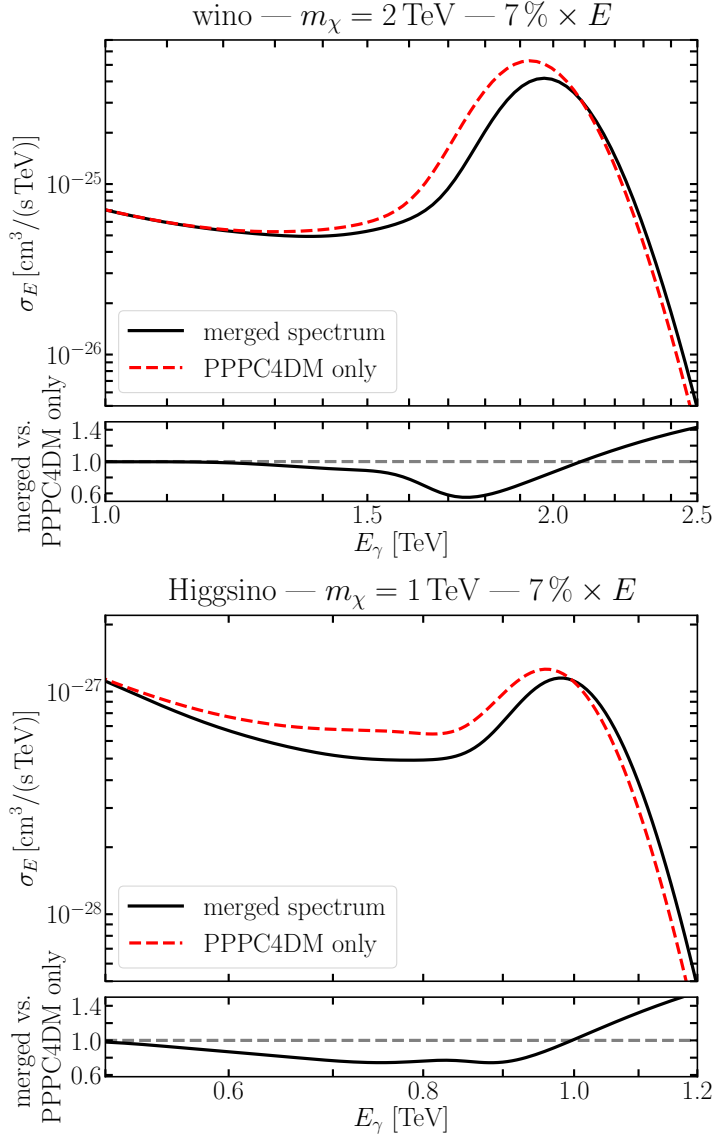


Figure 4: Mock folding with a Gaussian resolution of  $7\% \times E_\gamma$  of the spectra of Fig. 3 for the 2 TeV wino (upper panel), and 1 TeV Higgsino (lower panel). The merged endpoint-resummed spectrum is shown in black/solid, and the analogue PPC4DM-only spectrum (including NLO Sommerfeld enhancement) in red/dashed.

between resummation and Sommerfeld enhancement, when the Higgsino mass is of order and below 1 TeV, that further adds to this enhancement of the resummed spectrum at and beyond the endpoint [27].

For higher DM masses than those shown in Fig. 4, the differences between the PPC4DM prediction and the merged, resummed spectra are even more pronounced, as the resummed EW logarithms grow, and the large Sudakov suppression of the  $\chi^+\chi^-$  tree-level channel dominates the prediction.

In summary, we find that electroweak resummation significantly changes the shape of the photon energy spectrum in the range  $E_\gamma \sim (0.6 \dots 1) m_\chi$  and hence the form of the so-called “line-signal”. The present work demonstrates on the example of the wino and Higgsino model that an accurate matching of endpoint-resummed calculations to the full energy spectrum can be performed.

Ancillary to this paper, we provide the code `DM $\gamma$ Spec` that produces the merged differential spectra shown in Fig. 3 for DM masses in the range (0.5 – 100) TeV, together with other useful functions, such as cumulating the cross-section in energy bins. Furthermore, there is the option to use LO and NLO Sommerfeld calculations and different Higgsino mass splittings. A short description of the functionality is given in Appendix B.

## Acknowledgements

We thank Torsten Bringmann, Stefan Lederer and Clara Peset for useful discussions. This work has been supported in part by the DFG Collaborative Research Center “Neutrinos and Dark Matter in Astro- and Particle Physics” (SFB 1258).

## A Technical details

### A.1 Merging procedures

As the logarithms between narrow and intermediate resolution calculation match accurately for an extended region of  $1 - x$  [28], we merge the narrow and intermediate differential spectra according to

$$\left. \frac{d(\sigma v)}{dx} \right|_{\text{merged}} = w_1(x, \varepsilon) \left. \frac{d(\sigma v)}{dx} \right|_{\text{narrow}} + (1 - w_1(x, \varepsilon)) \left. \frac{d(\sigma v)}{dx} \right|_{\text{intermediate}} \quad (14)$$

with the simple linear function

$$w_1(x, \varepsilon) = \begin{cases} 0 & \text{if } \varepsilon < 1 - x \\ \frac{1}{1-4\varepsilon} \left(1 - \frac{1-x}{\varepsilon}\right) & \text{if } 4\varepsilon^2 \leq 1 - x \leq \varepsilon \\ 1 & \text{if } 1 - x < 4\varepsilon^2 \end{cases} \quad (15)$$

The merging starts at  $1 - x = 4\varepsilon^2$  in the center of the parametric validity region, and ends when the intermediate resolution calculation is fully valid at  $\varepsilon = 1 - x$ .

Based on the findings of Sec. 3, we devise a similar merging procedure between `PPPC4DM` and the intermediate calculation:

$$\left. \frac{d(\sigma v)}{dx} \right|_{\text{full merged}} = w_2(x, \varepsilon) \left. \frac{d(\sigma v)}{dx} \right|_{\text{merged}} + (1 - w_2(x, \varepsilon)) \left. \frac{d(\sigma v)}{dx} \right|_{\text{PPPC4DM}} \quad (16)$$

with

$$w_2(x, \varepsilon) = \begin{cases} 0 & \text{if } \min(20\varepsilon, 0.5) \leq 1 - x \leq 1 \\ 1 - \frac{1-x-\min(4\varepsilon, 0.2)}{\min(20\varepsilon, 0.5)-\min(4\varepsilon, 0.2)} & \text{if } \min(4\varepsilon, 0.2) \leq 1 - x \leq \min(20\varepsilon, 0.5) \\ 1 & \text{if } 0 \leq 1 - x \leq \min(4\varepsilon, 0.2) \end{cases} . \quad (17)$$

The boundaries for the start of merging the intermediate resolution and PPPC4DM are located well in the intermediate regime at  $\min(4\varepsilon, 0.2)$ . The value 0.2 is chosen, such that for small DM masses  $m_\chi < 10m_W$ , the merging region is extended. Similarly, we assign the upper value  $\min(20\varepsilon, 0.5)$  to the merging region beyond which the spectrum is fully determined by PPPC4DM.

Note that there is no overlap between the two merging steps for the DM masses relevant in this paper, as  $\min(4\varepsilon, 0.2) > \varepsilon$ , as long as  $m_\chi > 2.5m_W$ , i.e. for DM masses  $m_\chi > 200$  GeV.

## A.2 Zero-bin

In representing the spectra in the main text, we focused on the differential spectrum and excluded the absolute endpoint  $x = 1$  from the figures. The endpoint spectra are distribution-valued objects requiring careful treatment at the absolute endpoint. For example, the differential spectrum contains delta-distributions associated with the tree-level  $\chi\chi \rightarrow \gamma\gamma$  process and virtual corrections to this process, which are obviously not accessible in a plot of the result. In addition, the result depends on plus-distributions that arise from the expansion of

$$\frac{1}{(1-x)^{1-\eta}} = \frac{\delta(1-x)}{\eta} + \sum_{n=0}^{\infty} \frac{\eta^n}{n!} \left[ \frac{\ln^n(1-x)}{1-x} \right]_+ . \quad (18)$$

These contain subtractions if integrated to the endpoint. For example, for the ordinary plus-distribution

$$\int_0^1 d(1-x)f(1-x) \cdot \left[ \frac{1}{1-x} \right]_+ = \int_0^1 d(1-x) \frac{f(1-x) - f(0)}{1-x} . \quad (19)$$

To make the spectra easily accessible without having to worry about the implementation of the distributions, we provide in the code a zero-bin, which is the integral of the spectrum including  $\delta(1-x)$  terms from  $\chi\chi \rightarrow \gamma\gamma$  from the absolute endpoint  $x = 1$  to  $x = 1 - 2 \cdot 10^{-5}$ . The zero-bin takes care of all the distributions and their integration.

## A.3 Implementation of PPPC4DM

When using PPPC4DM [29] to merge with the endpoint-resummed spectra, we perform some modifications to obtain a consistent result. We exclude the tree-level final states  $\gamma\gamma, \gamma Z, ZZ$  in (3) (and therefore also their subsequent splittings) between the endpoint

and  $1 - x = 1 - 10^{-0.15}$  where effects of the otherwise smeared version of tree-level delta-distributions are visible. These tree-level pieces are part of the endpoint calculation, and hence to avoid double-counting need to be removed from PPC4DM. We confirmed analytically and numerically, following [37], that in this modified region, the neglected contributions are numerically subleading to the splitting  $dN_{WW}/dx$ .

In addition, we extend the interpolating tables provided by [29] for  $dN_{WW}/dx$  in the modified region discussed above, since the interpolating table is too sparse in the absolute endpoint region. To this end, we use the pure Monte Carlo data of [29] and apply the EW evolution following [37]. We confirm the few points provided by PPC4DM in this region and, by adding additional points to the interpolation, obtain a smooth interpolating function that is easily merged into the endpoint-resummed results.

## B Spectrum code – DM $\gamma$ Spec

Ancillary to this paper, we provide the code package DM $\gamma$ Spec that produces differential spectra (endpoint resummed to NLL' and merged to PPC4DM as discussed in the main text) and some other functions for the wino and Higgsino model in the DM mass range  $m_\chi = (0.5 - 100)$  TeV. Here we summarize the main functionality. A detailed account, including the code validation tests, is provided with the code in separate documentation at

`dmyspec.hepforge.org`

or alternatively from `https://users.ph.tum.de/t31software/dmyspec`. The code requires a Python 3 installation and the packages `numpy` and `scipy`. The main functions described below can be loaded with

```
from resummation import function_name
```

in a Python interpreter. Another (recommended) possibility is to use the provided example Jupyter notebook file (requires Jupyter notebooks installed), that can be loaded, e.g., via

```
jupyter notebook ./example_data.ipynb
```

in a Unix Shell. In the following, we describe the main functions of the code. An in-depth discussion including validation and further installation information can be found in the accompanying documentation on the webpage.

### B.1 diffxsection

Provides the differential cross-section  $d(\sigma v)/dx$  in  $x$  for  $\chi^0\chi^0 \rightarrow \gamma + X$  for all values of  $x$ , except for  $1 - x \leq 2 \cdot 10^{-5}$ , where the zero-bin at the absolute endpoint (see below) has to be used. The output of

$$\text{diffxsection}(x, \text{mchi}, \text{model}, \text{SF}) \tag{20}$$

has dimension  $10^{-26}\text{cm}^3/\text{s}$ . The function parameters refer to the variable  $\mathbf{x} = E_\gamma/m_\chi$ , and `mchi` to the DM mass in units of TeV. The parameter `model` specifies if the Higgsino or wino model shall be investigated, possible values are 'wino' or 'higgsino' (supplied as a Python string, i.e., including the quotation marks).

Finally there is the parameter `SF` that specifies the Sommerfeld-factor table to be used. The Sommerfeld factor, apart from the EW potential and the mass difference between partners in the multiplet, also depends on the velocity of the lightest DM particle, denoted by  $v$ . For the model 'wino', the identifier `SF` can take values from the list

'LO -3', 'LO -4', 'LO -5', 'NLO -3', 'NLO -4', 'NLO -5',

where either the LO or NLO Sommerfeld potential is used, and the negative integer  $n$  refers to the exponent of the (single-particle) velocity  $v = 10^n$ , at which the Sommerfeld enhancement is evaluated. The mass splitting between the charged and neutral wino is always fixed to  $\delta m_\chi = 164.1\text{ MeV}$ . For the model 'higgsino', the identifier `SF` can take the following 12 values:

'LO -3 dm 355 dmN 20', 'LO -4 dm 355 dmN 20', 'LO -5 dm 355 dmN 20',  
 'NLO -3 dm 355 dmN 20', 'NLO -4 dm 355 dmN 20', 'NLO -5 dm 355 dmN 20',  
 'LO -3 dm 355 dmN 015', 'LO -4 dm 355 dmN 015', 'LO -5 dm 355 dmN 015',  
 'NLO -3 dm 355 dmN 015', 'NLO -4 dm 355 dmN 015', 'NLO -5 dm 355 dmN 015'

The first two entries have the same interpretation as for the wino model. The number following `dm` specify the mass splitting between  $\chi_1^0$  and  $\chi^+$ , which always takes the value  $\delta m_\chi = 355\text{ MeV}$ . The last number specifies the mass difference between the two neutral Higgsinos  $\chi_1^0$  and  $\chi_2^0$ , and we provide tables for the two cases  $\delta m_N = 20\text{ MeV}$  and  $150\text{ keV}$ .

## B.2 cumulxsection

This function cumulates the cross section from the endpoint  $x = 1$  to a given  $x \leq 1$ , i.e.,

$$\int_{1-x}^1 dx' \frac{d(\sigma v)}{dx'}. \quad (21)$$

Note that if  $1 - x$  falls within the zero-bin, the integration is extended to the zero-bin size (see below). The output of

$$\text{cumulxsection}(\mathbf{x}, \text{mchi}, \text{model}, \text{SF}, \text{ZBsize} = \text{'default'}, \text{rel} = -3) \quad (22)$$

has dimension  $10^{-26}\text{cm}^3/\text{s}$  with function arguments as for `diffcross` above. In addition, there is the optional function value `ZBsize` that if omitted is set to 'default'. The possible parameters for this option are either 'default' corresponding to a zero-bin of width  $1 - x = 2 \cdot 10^{-5}$  or '1 %' for a zero-bin width of  $1 - x = 0.01$ . The parameter `rel` refers to the relative error requirement for the integrator and by default is set to `-3` corresponding to a relative error of  $10^{-3}$  (for an in-depth discussion, see the accompanying documentation).

### B.3 binnedcross

Similar function to `cumulcross` above, however, for a chosen energy bin from  $E_1$  to  $E_2$  with  $E_1 < E_2$ , i.e.,

$$\int_{E_1/m_\chi}^{E_2/m_\chi} dx \frac{d(\sigma v)}{dx}. \quad (23)$$

The output of

$$\text{binnedxsection}(\text{mchi}, E_1, E_2, \text{model}, \text{SF}, \text{ZBsize} = \text{'default'}, \text{rel} = -3) \quad (24)$$

has dimension  $10^{-26} \text{cm}^3/\text{s}$ , and the function parameters are as for `cumulcross` above, with the addition of  $E_1 < E_2 \leq m_\chi$  both given in units of TeV instead of `x`.

### B.4 zerobin

To allow for the inclusion of the absolute endpoint, at which the exclusive  $\chi\chi \rightarrow \gamma\gamma$  channel is located, a zero-bin has to be provided (cf. A.2). The zero-bin ranges are  $1 - x = 0$  to  $1 - x = 2 \cdot 10^{-5}$  (`'default'`) or to 0.01 (`'1 %'`). The output of

$$\text{zerobin}(\text{mchi}, \text{model}, \text{SF}, \text{ZBsize} = \text{'default'}) \quad (25)$$

has dimension  $10^{-26} \text{cm}^3/\text{s}$ . The function arguments are analogous to `cumulcross` above.

## References

- [1] N. Arkani-Hamed, A. Delgado and G. F. Giudice, *The well-tempered neutralino*, *Nucl. Phys. B* **741** (2006) 108–130 [[hep-ph/0601041](#)].
- [2] M. Cirelli, N. Fornengo and A. Strumia, *Minimal dark matter*, *Nucl. Phys. B* **753** (2006) 178–194 [[hep-ph/0512090](#)].
- [3] M. Cirelli, A. Strumia and M. Tamburini, *Cosmology and Astrophysics of Minimal Dark Matter*, *Nucl. Phys. B* **787** (2007) 152–175 [[0706.4071](#)].
- [4] M. Beneke, C. Hellmann and P. Ruiz-Femenía, *Heavy neutralino relic abundance with Sommerfeld enhancements - a study of pMSSM scenarios*, *JHEP* **03** (2015) 162 [[1411.6930](#)].
- [5] M. Beneke, R. Szafron and K. Urban, *Sommerfeld-corrected relic abundance of wino dark matter with NLO electroweak potentials*, *JHEP* **02** (2021) 020 [[2009.00640](#)].
- [6] A. Canepa, T. Han and X. Wang, *The Search for Electroweakinos*, *Ann. Rev. Nucl. Part. Sci.* **70** (2020) 425–454 [[2003.05450](#)].

- [7] R. K. Ellis *et. al.*, *Physics Briefing Book: Input for the European Strategy for Particle Physics Update 2020*, 1910.11775.
- [8] Q. Chen and R. J. Hill, *Direct detection rate of heavy Higgsino-like and Wino-like dark matter*, *Phys. Lett. B* **804** (2020) 135364 [1912.07795].
- [9] **HESS** Collaboration, H. Abdallah *et. al.*, *Search for  $\gamma$ -Ray Line Signals from Dark Matter Annihilations in the Inner Galactic Halo from 10 Years of Observations with H.E.S.S.*, *Phys. Rev. Lett.* **120** (2018), no. 20 201101 [1805.05741].
- [10] **CTA** Collaboration, A. Acharyya *et. al.*, *Sensitivity of the Cherenkov Telescope Array to a dark matter signal from the Galactic centre*, *JCAP* **01** (2021) 057 [2007.16129].
- [11] L. Bergstrom and P. Ullio, *Full one loop calculation of neutralino annihilation into two photons*, *Nucl. Phys. B* **504** (1997) 27–44 [hep-ph/9706232].
- [12] Z. Bern, P. Gondolo and M. Perelstein, *Neutralino annihilation into two photons*, *Phys. Lett. B* **411** (1997) 86–96 [hep-ph/9706538].
- [13] P. Ullio and L. Bergstrom, *Neutralino annihilation into a photon and a Z boson*, *Phys. Rev. D* **57** (1998) 1962–1971 [hep-ph/9707333].
- [14] J. Hisano, S. Matsumoto and M. M. Nojiri, *Explosive dark matter annihilation*, *Phys. Rev. Lett.* **92** (2004) 031303 [hep-ph/0307216].
- [15] J. Hisano, S. Matsumoto, M. M. Nojiri and O. Saito, *Non-perturbative effect on dark matter annihilation and gamma ray signature from galactic center*, *Phys. Rev. D* **71** (2005) 063528 [hep-ph/0412403].
- [16] M. Beneke, C. Hellmann and P. Ruiz-Femenía, *Non-relativistic pair annihilation of nearly mass degenerate neutralinos and charginos III. Computation of the Sommerfeld enhancements*, *JHEP* **05** (2015) 115 [1411.6924].
- [17] M. Beneke, R. Szafron and K. Urban, *Wino potential and Sommerfeld effect at NLO*, *Phys. Lett.* **B800** (2020) 135112 [1909.04584].
- [18] K. Urban, *NLO electroweak potentials for minimal dark matter and beyond*, *JHEP* **10** (2021) 136 [2108.07285].
- [19] M. Baumgart, T. Cohen, I. Mould, N. L. Rodd, T. R. Slatyer, M. P. Solon, I. W. Stewart and V. Vaidya, *Resummed Photon Spectra for WIMP Annihilation*, *JHEP* **03** (2018) 117 [1712.07656].
- [20] M. Beneke, A. Broggio, C. Hasner and M. Vollmann, *Energetic  $\gamma$ -rays from TeV scale dark matter annihilation resummed*, *Phys. Lett. B* **786** (2018) 347–354 [1805.07367]. [Erratum: Phys.Lett.B 810, 135831 (2020)].

- [21] M. Baumgart, I. Z. Rothstein and V. Vaidya, *Constraints on Galactic Wino Densities from Gamma Ray Lines*, *JHEP* **04** (2015) 106 [1412.8698].
- [22] M. Baumgart, I. Z. Rothstein and V. Vaidya, *Calculating the Annihilation Rate of Weakly Interacting Massive Particles*, *Phys. Rev. Lett.* **114** (2015) 211301 [1409.4415].
- [23] M. Bauer, T. Cohen, R. J. Hill and M. P. Solon, *Soft Collinear Effective Theory for Heavy WIMP Annihilation*, *JHEP* **01** (2015) 099 [1409.7392].
- [24] G. Ovanessian, T. R. Slatyer and I. W. Stewart, *Heavy Dark Matter Annihilation from Effective Field Theory*, *Phys. Rev. Lett.* **114** (2015), no. 21 211302 [1409.8294].
- [25] G. Ovanessian, N. L. Rodd, T. R. Slatyer and I. W. Stewart, *One-loop correction to heavy dark matter annihilation*, *Phys. Rev. D* **95** (2017), no. 5 055001 [1612.04814]. [Erratum: *Phys.Rev.D* 100, 119901 (2019)].
- [26] M. Baumgart, T. Cohen, E. Moulin, I. Moutl, L. Rinchuso, N. L. Rodd, T. R. Slatyer, I. W. Stewart and V. Vaidya, *Precision Photon Spectra for Wino Annihilation*, *JHEP* **01** (2019) 036 [1808.08956].
- [27] M. Beneke, C. Hasner, K. Urban and M. Vollmann, *Precise yield of high-energy photons from Higgsino dark matter annihilation*, *JHEP* **03** (2020) 030 [1912.02034].
- [28] M. Beneke, A. Broggio, C. Hasner, K. Urban and M. Vollmann, *Resummed photon spectrum from dark matter annihilation for intermediate and narrow energy resolution*, *JHEP* **08** (2019) 103 [1903.08702]. [Erratum: *JHEP* 07, 145 (2020)].
- [29] M. Cirelli, G. Corcella, A. Hektor, G. Hutsi, M. Kadastik, P. Panci, M. Raidal, F. Sala and A. Strumia, *PPPC 4 DM ID: A Poor Particle Physicist Cookbook for Dark Matter Indirect Detection*, *JCAP* **03** (2011) 051 [1012.4515]. [Erratum: *JCAP* 10, E01 (2012)].
- [30] M. Beneke, S. Lederer and C. Peset, in preparation.
- [31] Y. Yamada, *Electroweak two-loop contribution to the mass splitting within a new heavy  $SU(2)_L$  fermion multiplet*, *Phys. Lett. B* **682** (2010) 435–440 [0906.5207].
- [32] M. Ibe, S. Matsumoto and R. Sato, *Mass Splitting between Charged and Neutral Winos at Two-Loop Level*, *Phys. Lett.* **B721** (2013) 252–260 [1212.5989].
- [33] S. D. Thomas and J. D. Wells, *Phenomenology of Massive Vectorlike Doublet Leptons*, *Phys. Rev. Lett.* **81** (1998) 34–37 [hep-ph/9804359].

- [34] C. W. Bauer, S. Fleming, D. Pirjol and I. W. Stewart, *An Effective field theory for collinear and soft gluons: Heavy to light decays*, *Phys. Rev. D* **63** (2001) 114020 [[hep-ph/0011336](#)].
- [35] C. W. Bauer, D. Pirjol and I. W. Stewart, *Soft collinear factorization in effective field theory*, *Phys. Rev. D* **65** (2002) 054022 [[hep-ph/0109045](#)].
- [36] M. Beneke, A. P. Chapovsky, M. Diehl and T. Feldmann, *Soft collinear effective theory and heavy to light currents beyond leading power*, *Nucl. Phys. B* **643** (2002) 431–476 [[hep-ph/0206152](#)].
- [37] P. Ciafaloni, D. Comelli, A. Riotto, F. Sala, A. Strumia and A. Urbano, *Weak Corrections are Relevant for Dark Matter Indirect Detection*, *JCAP* **03** (2011) 019 [[1009.0224](#)].
- [38] L. Bergstrom, T. Bringmann, M. Eriksson and M. Gustafsson, *Gamma rays from heavy neutralino dark matter*, *Phys. Rev. Lett.* **95** (2005) 241301 [[hep-ph/0507229](#)].